JCI The Journal of Clinical Investigation

Suppressing the DSCAM/PAK1 pathway reverses neurogenesis deficits in Down Syndrome patient iPSC-derived cerebral organoids

Xiao-Yan Tang, … , Mingyan Lin, Yan Liu

J Clin Invest. 2021. https://doi.org/10.1172/JCI135763.

Research In-Press Preview Neuroscience Stem cells

Graphical abstract

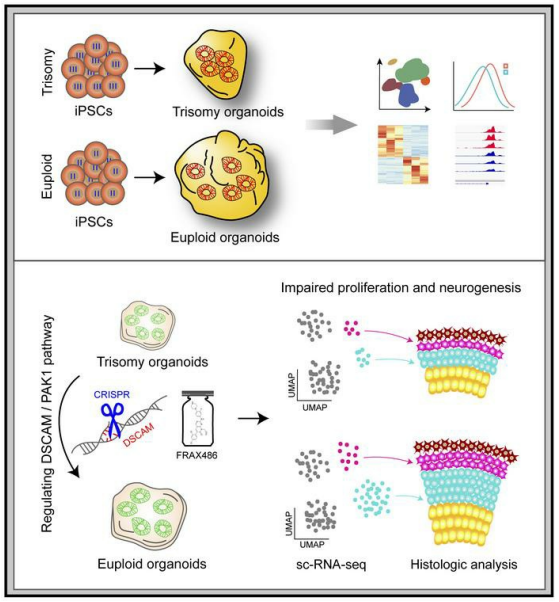

Suppressing the DSCAM/PAK1 pathway reverses neurogenesis deficits in Down Syndrome patient iPSC-derived cerebral organoids.

Xiao-Yan Tang [1], Lei Xu[1], Jingshen Wang[2], Yuan Hong[1], Yuanyuan Wang[2], Qian Zhu[1], Da Wang[1], Xin-Yue Zhang [1], Chun-Yue Liu[2], Kai-Heng Fang[1], Xiao Han[1], Shihua Wang[3], Xin Wang[3], Min Xu[1], Anita Bhattacharyya[4,5], Xing Guo[2, 6]*, Mingyan Lin[2]*, Yan Liu[1]*

1 Institute for Stem Cell and Neural Regeneration, State Key Laboratory of Reproductive Medicine, School of Pharmacy, Nanjing Medical University, Nanjing, China, 211166

2 Department of Neurobiology, School of Basic Medical Sciences, Nanjing Medical University, Nanjing, Jiangsu 211166, China

3 State Key Laboratory of Cellular Stress Biology, Fujian Provincial Key Laboratory of Neurodegenerative Disease and Ageing Research, Institute of Neuroscience, School of Medicine, Xiamen University, Xiamen, China, 361102

4 Waisman Center, University of Wisconsin, Madison, WI, USA, 53705

5 Department of Cell and Regenerative Biology, School of Medicine and Public Health, University of Wisconsin, Madison, WI, USA, 53705

6 Department of Endocrinology, Sir Run Run Hospital, Nanjing Medical University, Nanjing, Jiangsu, China

*Correspondence: yanliu@njmu.edu.cn (Y. Liu), linmingyan@njmu.edu.cn (M. Lin), and guox@njmu.edu.cn (X. Guo)

Declaration of interests

The authors declare no competing interests.

Abstract

Down syndrome (DS), caused by trisomy of chromosome 21, occurs in 1 of every 800 live births. Early defects in cortical development likely account for the cognitive impairments in DS, although the underlying molecular mechanism remains elusive. Here, we performed histological assays and unbiased single-cell RNA sequencing (scRNA-seq) analysis on cerebral organoids derived from four euploid cell lines and from induced pluripotent stem cells (iPSCs) from three individuals with trisomy 21 to explore cell type-specific abnormalities associated with DS during early brain development. We found that neurogenesis was significantly affected based on diminished proliferation and decreased expression of layer II and IV markers in cortical neurons in the subcortical regions; this may be responsible for the reduced size of the organoids. Furthermore, suppression of the DSCAM-PAK1 pathway which showed enhanced activities in DS) via CRISPR/Cas9, CRISPRi or small-molecule inhibitor treatment reverses abnormal neurogenesis, thereby increasing the size of organoids derived from DS iPSCs. Our study demonstrated that 3D cortical organoids developed in vitro are a valuable model of DS and provided a direct link between dysregulation of the DSCAM-PAK1 pathway and developmental brain defects in DS.

Key words: induced pluripotent stem cell, differentiation, Down syndrome, cerebral organoids, cortical development, trisomy 21

Introduction

Down syndrome (DS), caused by trisomy of chromosome 21, is the most frequent genetic cause of birth defects and cognitive abnormalities, with an occurrence of 1 of 800 live births (1). Decades of research using transgenic mouse models and postmortem human tissues have revealed that the characteristics of DS include reduced brain weight, cerebral atrophy, thinner cortex, impaired neurogenesis and altered cortical lamination (2-6). Moreover, in vitro culture of neural progenitor cells (NPCs) isolated from DS fetuses revealed impaired proliferation (7) and reduced neurogenesis (8-10), which was informative in dissecting the mechanisms underlying early brain defects in DS. Nevertheless, the above results were based on inaccessible pathological specimens, so there is a need to better clarify the pathogenesis of DS by using a readily available model of human origin. The advent of human induced pluripotent stem cells (iPSCs) presents unprecedented opportunities to establish human cellular models for investigating neurodevelopmental diseases. Using human PSC technology, our previous reports have demonstrated that DS iPSC-derived neurons displayed significant synaptic deficits (11) as well as impaired migration and neurite projection (12). Despite the accumulated knowledge in the past two decades regarding neural development in DS, the mechanisms underlying impaired cortical development in DS are still unclear.

Recent advances in cerebral organoid culture systems have opened new avenues to study human developmental disorders (13-24). Cerebral organoids are three-dimensional (3D) structures reminiscent of human brain regions, including the cerebral cortex and subventricular zone. Recently, several independent studies have established cerebral organoids to clarify the pathogenesis of microcephaly, autism, Miller-Dieker syndrome and other neurodevelopmental disorders (14, 15, 20, 21, 25-29), but there have been no reports on the pathological mechanism underlying delayed

cortical development in DS.

Among the protein-coding genes in HSA21 (human chromosome 21), Down's syndrome cell adhesion molecule (DSCAM) encodes a cell adhesion molecule involved in neuronal generation, maturation, dendrite morphology and neuronal wiring (30) (31), which is important for brain development. Triplication of the DSCAM gene deregulated the activity of PAK1 and pPAK1, resulting in neuronal connectivity dysfunction in immortalized cells from trisomy 16 (Ts16) fetal mice (32). PAK1, a gene downstream of DSCAM, plays a role in cortical development by regulating the proliferation of neural progenitors (33). Nevertheless, it is unclear whether the DSCAM-PAK1 pathway regulates the development of the cerebral cortex in DS.

Here, we established 3D cerebral organoid culture to investigate the mechanisms associated with abnormal cerebral development in DS. To resolve confounding factors owing to the asynchronous and heterogeneous appearance of disease phenotypes in in vitro culture, we performed high-resolution single-cell transcriptomic analyses to uncover the cell-type-specific molecular pathology of DS. Our data showed that DS iPSC-derived cerebral organoids partially recapitulated the abnormalities observed in DS mouse models and postmortem DS brain samples, including a reduced proliferation rate and abnormal neurogenesis. Furthermore, we showed that thinner cortex and proliferation deficits in DS organoids could be reversed by knocking out one locus of the three DSCAM alleles. Likewise, the small-molecule inhibitor FRAX486 could rescue the neuropathological phenotypes by regulating the expression of PAK1. Our findings may provide a potential target for prenatal intervention for DS.

Results

Single-cell RNA-seq revealed altered neural development in trisomy 21 organoids

To generate organoids from human PSCs, we modified the protocol of cerebral organoid generation from previous reports (34-37) (Figure 1A, Supplemental Figure 1). After continuous culture for 30-60 days, the cerebral organoids displayed stratified neuroepithelium-like architecture expressing neural progenitor markers at day 30 and cortical layer markers at days 50-70 (Supplemental Figure 1). Moreover, the cortical upper-layer markers could be examined after 100-115 days of differentiation (Supplemental Figure 1).

Next, we generated organoids from three iPSC lines from three DS patients (DS1, 2DS3, and DSP), three euploid iPSC lines (IMR90-4, ihtc-03, and DS2U), and one hESC line (H9) (Figure 1A). Similar to euploid organoids, trisomy 21 organoids displayed regionalization and cortical layers (Figure 1, B-D). To gain insight into the cell-type-specific transcriptomic changes in trisomy and euploid organoids, we profiled cerebral organoids (n=65,342 cells from 7 hPSC lines) at day 30 and day 70 using 10X Genomics Chromium Single Cell RNA Sequencing (Figure 1A, Supplemental Table 3). Unbiased clustering identified eight major cell types (Figure 1E), which were then annotated according to the expression of known cell-type markers (Supplemental Figure 2A). To verify the regional identity of cells in cerebral organoids, we mapped the scRNA-seq data onto 3D in situ hybridization data from the Allen Brain Atlas by using the VoxHunt algorithm. We found that clusters in cerebral organoids highly mapped onto the dorsal forebrain of the embryonic day (E) 13.5 mouse brain (Figure 1F). In addition, our samples showed a maximum correlation with transcriptomes from post-conceptual week (pcw) 8 to pcw 16 samples of the developing human brain (Supplemental Figure 2B). We then compared our scRNA-seq transcriptome data with the BrainSpan database. Remarkably, organoids showed a significant positive correlation with postmortem fetal tissues at pcw 8 and 9 (Figure 1J). By comparing the proportion of cells in each cluster, we found that cell diversity was similar across lines and groups (Supplemental Figure 2C). The box plot between pseudotime and subclusters supported our speculation that developmental stage classification was positively correlated with pseudotime (Supplemental Figure 2D), while a delayed developmental state from the progenitor-to-neuron trajectory was found in trisomy 21

organoids in comparison with the developmental state of euploid organoids at 30 days (Figure 1, H and I). Gene ontology (GO) analysis showed that the significantly differentially expressed genes (DEGs) among all the clusters were enriched in biological processes such as neurogenesis, forebrain development and neural precursor cell proliferation (Figure 1J). Consistent with this, pathway enrichment analyses indicated that neurogenesis-related pathways were significantly altered (Supplemental Figure 2E).

Taken together, these data show that neural development in the DS cerebral organoids exhibited significant alterations compared to that in euploid organoids.

Disrupted chromatin accessibility underlies impaired transcription in cerebral organoids derived from trisomy iPSCs

Large genomic changes can result in the disruption of several aspects of chromatin conformation (38), such as the distribution of chromatin accessibility. To test whether global chromatin accessibility was affected in DS, we profiled the genome-wide chromatin accessibility of day 30 cerebral organoids by using ATAC-seq. In general, the distribution of chromatin accessibility remained unchanged in DS (Supplemental Figure 3A). However, dramatic and widespread increases in chromatin accessibility were observed across the promoter regions of chromosome 21 in DS, which conformed with the characteristics of trisomy 21 (Figure 2, A and B). Many regions on other chromosomes also showed significant changes in accessibility, with 1785 increased and 1695 decreased differentially open chromatin regions (dOCRs) identified in organoids derived from trisomy iPSCs compared to those derived from euploid iPSCs (Figure 2C). Among them, OCRs associated with the markers *PAX6, GLPER, PTCH1, LMO1, VCAM1* and *WNT7A* showed a decrease in chromatin openness at their promoters in the trisomy samples (Supplemental Figure 3B). By identifying the transcription factor motifs enriched in the trisomy- and euploid-specific accessible regions, we found that many genes regulated by SOX2, lsl1 and Rfx5 had decreased

accessibility in the trisomy samples (Supplemental Figure 3C). This result was consistent with our findings that genes near dOCRs were enriched in neurogenesis and nervous system development (Supplemental Figure 3D).

To examine whether disruption of chromatin accessibility would be responsible for transcriptomic changes, we performed bulk RNA-seq analyses of day 30 cerebral organoids in the two groups. Differential expression profiling of 104 upregulated genes and 91 downregulated genes is displayed as a heatmap (Figure 2D, Supplemental Table 5). Consistent with the findings of the scRNA-seq data, the DEGs between the trisomy- and euploid-derived organoids showed significant enrichment of genes related to nervous system development, cell proliferation and neurogenesis (Supplemental Figure 3, E and F; Supplemental Table 6 and 7). Notably, the expression of Ki67 and PAX6, which are involved in regulating proliferation, was decreased in the trisomy organoids (Supplemental Figure 3, G and H). We then mapped the 20 differentially expressed proteins related to neurogenesis and 29 related to cell proliferation by using the STRING database (Supplemental Figure 3I). Not surprisingly, we observed a positive correlation between the change in a differentially accessible peak and the fold change in expression of its nearest gene (Spearman coefficient r = 0.165) (Figure 2E). GO analyses of the co-ordinately upregulated and downregulated genes were enriched among biological processes such as central nervous system neuron differentiation, neuron migration and glutamate receptor signalling pathway (Figure 2F).

Taken together, these results suggested that at least part of transcriptomic changes in DS are linked to the altered accessibility of their adjacent chromatin.

Reduced proliferation of NPCs resulted in smaller size of DS-derived cortical organoids

To verify the neuropathological phenotypes observed in the RNA-seq data, we compared the proliferation of DS and control organoids. Strikingly, in contrast to euploid embryonic bodies on day 7, trisomy embryonic bodies showed a reduced perimeter length (Figure 3, A and B). Moreover, the size of the trisomy 21 organoids was obviously smaller than that of the euploid organoids and

exhibited significantly decreased expansion rates (Figures 3, C and D, Supplemental Figure 4C). To further examine the abnormal structures in day 30 trisomy 21 organoids, we assessed the architecture of neuroepithelial loops with respect to the length of the apical and basal membranes, the diameter of the loops and the size of the ventricle-like area, total loop area, and loop tissue area in the trisomy and euploid organoids (Figure 3E). We found that compared to the euploid organoids, the trisomy 21 organoids exhibited a reduction in all parameters (Figure 3, F-K). This phenotype is consistent with previous observations of a reduction in brain size in DS patients (2, 4-6).

Defects in proliferation during early neural development could influence the size of the forebrain (39) (40). To test whether altered proliferation of VZ NPCs may delay the organoid expansion of trisomy, the percentages of $Ki67^+$, EdU^+ and $PAX6^+$ cells in the VZ-like region were quantified at 30 days after differentiation initiation (Figure 4, A-C; Figure 4, E-G). In accordance with the reduction in organoid size, we found not only markedly decreased proliferation in the trisomy cortical VZ-like regions but also fewer $SOX2^+$ progenitor cells located in the region (day 30: DS1, 83.76%±1%; 2DS3, 82.31% ± 1.02%; DSP, 81.96% ± 0.88%; DS2U, 90.01%±0.77%; ihtc-03, 88.53%±0.77%; IMR90-4, 88.16% ± 0.77%; and H9, 88.79% ± 0.90%; Figure 4, D and H), whereas the expression of apoptosis markers was not significantly altered at the same time point (Supplemental Figure 4, D and E). These results suggested that decreased proliferation of trisomy NPCs was responsible for the smaller size of the trisomy 21 organoids.

We next assessed the generation of different subtypes of cortical neurons by using the validated markers at 50 days after differentiation initiation. The percentage of $CTIP2^+$ cells was decreased in the DS group compared to the euploid control group (DS1, 17.01%±1.87%; IMR90-4, 31.1% ± 2.17%), while the percentage of $TBR1^+$ cells was unchanged (Supplemental Figure 4, F-H). To

further study the later developmental stages in DS, we performed scRNA sequencing and histological analysis in day 70 cerebral organoids (Figure 5A). Uniform manifold approximation and projection (UMAP) visualization of subclusters of glutamatergic neurons showed that the composition of cortical mature deep-layer and mature upper-layer neurons was dramatically decreased in the trisomy 21 organoids (Figure 5, B and C). Moreover, the proportion of cells expressing cortical upper-layer markers, such as BRN2 and SATB2, was decreased in trisomy glutamatergic neurons (Figure 5D). Indeed, our histology results showed that the percentages of $CTIP2^+$ and $SATB2^+$ cells were significantly decreased at 70 days in the DS-derived organoids, which was consistent with the gene expression profile (CTIP2: DS1, 21.87%±1.63%; IMR90-4, 40.13%±2.1%; SATB2: DS1, 9.23%±1.03%; IMR90-4, 15.75% ± 0.5%; Figure 5, E-H).

Taken together, these results suggested that decreased proliferation might contributes to reduced neurogenesis in trisomy 21 organoids.

Knockdown of *DSCAM* reversed defects of proliferation in DS organoids

Previous studies have demonstrated that *DSCAM* is significantly overexpressed in postmortem tissues from individuals with DS (41) and animal models of DS (42-44). In line with previous studies, we found that *DSCAM* expression was increased in cells with trisomy 21, as assessed by quantitative real-time polymerase chain reaction (qPCR) (Figure 6A). Meanwhile, OCRs of the marker *DSCAM* also showed a marked increase in chromatin openness at their promoters in trisomy 21 organoids (Figure 6B). Strikingly, we observed that the protein levels of DSCAM in DS were also significantly higher than those in the controls (Figure 6, D and F). PAK1 regulates the proliferation of neural progenitors (33) and synaptic plasticity as the downstream of DSCAM (32), which prompted us to

probe the expression levels of PAK1. Indeed, qPCR analysis showed a higher level of *PAK1* mRNA in trisomy cells than in euploid control cells (Figure 6C), which was consistent with the observed protein level (Figure 6, D and G). In addition, the protein level of phosphorylated PAK1 (p-PAK1) was substantially increased in DS organoids compared with euploid organoids (Figures 6, E and H). These results show that the DSCAM-PAK1 pathway was altered in trisomy 21 organoids.

We then hypothesized that the defects of neurogenesis in DS observed in vitro is attributed to altered expression of DSCAM and its downstream protein PAK1. To test this hypothesis, we used CRISPR/Cas9 genome editing to establish DSCAM-KD iPSCs from the DS1 iPSC line (Figure 6I and Supplemental Figure 5A), followed by differentiation of the DS and edited iPSC lines (named DSCAM-KD$^{2\text{-}1\text{-}6}$ and DSCAM-KD$^{2\text{-}1\text{-}12}$) into cerebral cortical organoids. Karyotype analysis of DS and DSCAM-KD iPSC-derived organoids showed trisomy of HSA21 (Supplemental Figure 5B). scRNA expression profiling of DSCAM-KD cerebral organoids at 30 days after induction of differentiation showed that there was a positive correlation in the changes in expression between DSCAM-KD organoids and euploid organoids with respect to trisomy, which indicates the successful restoration of the transcriptome in DSCAM-KD (Figure 6J). In addition, we noticed that the mean expression levels of genes downregulated in DS were restored in the DSCAM-KD groups to levels similar to those in the euploid groups (Figure 6K). Further analysis showed that the mean expression level of *DSCAM* was significantly downregulated in subclusters of DSCAM-KD cerebral organoids compared to DS1 cerebral organoids (Figure 6L).

Specifically, the protein expression levels of DSCAM, PAK1 and p-PAK1 were decreased in the DSCAM-KD groups compared to the DS1 group (Figure 6, M-Q). These results confirmed the efficient knockdown of *DSCAM* in the DSCAM-KD$^{2\text{-}1\text{-}6}$ and DSCAM-KD$^{2\text{-}1\text{-}12}$ groups, with a

prominent and consistent reduction at both the RNA and protein levels. Furthermore, we observed a partial rescue in all parameters in DSCAM-KD organoids compared to DS1 organoids (Figure 7, A-C, Supplemental Figure 5, C-E).

Next, we examined whether a reduction in *DSCAM* gene dosage in DS1 organoids could rescue the proliferation deficits observed in dorsal neural progenitors. Remarkably, we found that there was increased expression of Ki67, PAK6 and SOX2 in the VZ-like region in the DSCAM-KD groups (Figure 7, D and E), suggesting enhanced proliferation upon knocking down *DSCAM*. Importantly, the reduced DSCAM gene dosage in the trisomy 21 organoids restored the numbers of $CTIP2^{+}$ neurons (DS1: 17.11%±1.20%; $DSCAM\text{-}KD^{2\text{-}1\text{-}12}$: 26.86%±1.62%; $DSCAM\text{-}KD^{2\text{-}1\text{-}6}$: 26.88%±1.62%) and $SATB2^{+}$ neurons (DS1: 10.14%±0.76%; $DSCAM\text{-}KD^{2\text{-}1\text{-}12}$: 16.54%±1.44%) to numbers similar to those in the euploid organoids (Figure 7, F-I).

To confirm the effects of DSCAM in DS, we further downregulated *DSCAM* in DS1 by carrying out a CRISPR interference (CRISPRi) experiment (Supplemental Figure 6, A-D). The expression levels of DSCAM, PAK1 and p-PAK1 were robustly increased in DSCAM-KD cerebral organoids (Supplemental Figure 6, E-G). Furthermore, the perimeter of day 7 embryonic bodies, the size of the VZ zone in the organoids, cell proliferation and cortical neurogenesis were effectively elevated in the CRISPRi-based DSCAM-KD groups (Supplemental Figure 7, A-H).

Taken together, these results demonstrated that the proliferation and neurogenesis deficits in trisomy 21 organoids can be rescued by regulating the *DSCAM* gene.

FRAX486 rescued the abnormal proliferation and neurogenesis of DS organoids

Considering that the DSCAM-PAK1 pathway is involved in neurodevelopment and is altered in DS

(32, 33), we investigated whether the defects could be rescued by applying small molecules targeting this pathway (Figure 8A). Indeed, pre-treatment of DS1 organoids with FRAX486, an inhibitor that regulates the phosphorylation of PAK1, reduced the protein levels of p-PAK1 (Figures 8, B and D) without changing the expression levels of total PAK1 (Figure 8, C and E). Of note, we did not find significant changes in the protein levels of PAK1 and p-PAK1 in euploid organoids that were pre-treated with FRAX486 (Supplemental Figure 8, A-H). Furthermore, we tested whether the inhibition of PAK1 with FRAX486 could ameliorate the defective neurogenesis of DS organoids. Indeed, we observed a partial rescue in the abnormal architecture of neuroepithelial loops (Figure 8, F and G, Supplemental Figure 8, I-K). In addition, FRAX486 effectively increased the proliferation of NPCs after 30 days of differentiation (Ki67: DS1, 18.32%±2.19%; DS1+FRAX, 24.85%±0.95%; PAX6: DS1, 70.05%±3.84%; DS1+FRAX, 81.50%±1.13%; and SOX2: DS1, 81.14%±0.97%; DS1+FRAX, 90.01%±0.77%; Figure 8, H and I). Furthermore, PAK1 inhibition via FRAX486 treatment subsequently increased the expression of CTIP2 (50 days after initiation of differentiation, DS1: 17.37%±1.11%; DS1+FRAX: 27.92%±1.67%) and SATB2 (70 days after initiation of differentiation, DS1, 11.17%±0.6%; DS1+FRAX, 14.57%±0.75%), suggesting the rescue of neurogenesis (Figure 8, J-M).

Discussion

In this study, we studied cortical developmental defects in DS by using a patient iPSC-derived cerebral organoid model. The DS organoids showed reduced proliferation in the VZ, decreased neuron distribution in the cortical plate and smaller cerebral organoids. Transcriptomic and western blot results revealed that DSCAM and PAK1 may play roles in contributing to these defects. Moreover, genetic correction and treatment with a small-molecule inhibitor targeting of the DSCAM-PAK1 pathway rescued the neurogenesis deficits.

A recent study using DS iPSCs reported that overexpression of OLIG2 in DS cells may cause overproduction of subclass-specific GABAergic interneurons (primarily CR^+ and SST^+ neurons), which might contribute to intellectual disabilities related to trisomy 21 (45); however, this work did not mention cortical development in DS. Early studies using DS postmortem tissue have demonstrated that DS individuals exhibit a 20-50% reduction in neurons in the granular layers (2, 46, 47). In addition, subsequent studies on DS fetal brains described fewer neurons (20-50% less than control) and a significant reduction in brain weight at pcw 15 (6, 48). These observations suggested impaired neurogenesis in the cortex during prenatal neurodevelopment. In line with this hypothesis, we demonstrated reduced proliferation of progenitors and a subsequent reduction in the number of cortical neurons expressing markers corresponding to layers IV and II (Figure 4, A-H; Figure 4, L-O; Supplemental Figure 7, F and H). These observations provide evidence of impaired neurogenesis of cortical neurons that may underlie the reduced cortical size of the brain in individuals with DS.

Many attempts have been made to investigate HSA21 genes associated with neurological defects in DS (49, 50). However, the molecular mechanisms underlying smaller brain sizes remain

unknown. Our transcript profiling indicated that multiple neurogenesis pathways were altered in the cerebral organoids derived from DS iPSCs. We focused on the DSCAM pathway and showed that DSCAM expression was upregulated in DS iPSC-derived cerebral organoids. DSCAM is critical for neurodevelopment in flies and mice (32, 51), but its role in human brain development is poorly understood. Strikingly, our western blot analysis revealed increased DSCAM expression in cerebral organoids derived from iPSCs from DS patients. Overexpression of DSCAM in neurons from a mouse model of DS could deregulate the activity of its downstream gene PAK (32). Indeed, we found abnormal activation of PAK1 and p-PAK1 in the DS groups, which may be partially responsible for the neurogenesis defects in DS.

Recently, *DSCAM* has received increasing attention due to its implication in neurodevelopment, but the function of DSCAM in NPCs is not entirely known. Prior work has revealed that knocking down *DSCAM* increases the complexity of proximal dendritic branching and inhibits axon growth in mouse cortical neurons (52). However, its role in cortical neurogenesis in primates has not been studied. Its downstream gene *PAK1* has been reported to play an essential role in regulating actin cytoskeleton dynamics, dendritic spine morphogenesis and cortical neurogenesis in a mouse model (33, 53). Here, we used both genetic correction and small-molecule inhibitors to rescue proliferation and neurogenesis defects in DS organoids. Our work indicated that the DSCAM-PAK1 pathway may play a role in regulating proliferation and neurogenesis, which might be associated with the abnormal development of DS neurons.

Our cerebral organoid models provide a new avenue to study the early developmental deficits in DS. By using transcriptomic analysis, CRISPR-based gene correction, and small-molecule intervention, we demonstrated that the malformation of cortical development in DS was attributed

to reduced neuronal proliferation of progenitors and was accompanied by neurogenesis deficits. Among them, dysfunction of the DSCAM-PAK1 pathway has been shown to play a critical role in the pathogenesis of DS. On the one hand, our current analyses provide candidates for identifying therapeutic targets and screening drugs for DS. Moreover, DSCAM and PAK1 are potential therapeutic targets to reverse abnormal neurodevelopment and improve postnatal cognitive function in DS.

Methods

iPSC culture and generation of organoids. Trisomy 21 iPSC lines (DS1, 2DS3, and DSP) and euploid iPSC lines (IMR90-4, H9, DS2U and ihtc-03) were used in this study (detailed list in Supplemental Table 1). DS iPSC lines were generated from two DS patients as reported by Weick et al (11) or from a mosaic DS individual. The euploid iPSC lines DS2U (the euploid control was from the same patient with DS1), wild-type IMR90-4 (WiCell Agreement NO. 17-W0063), ihtc-03 (established in our laboratory) and the hESC line H9 (WiCell Agreement NO. 16-W0060) served as euploid controls. iPSC lines were maintained under feeder-free conditions by coating the culture plates with vitronectin (Thermo Fisher Scientific) as described in our previous studies (35). After 5-7 days of culture in E8 medium (Thermo Fisher Scientific), hPSCs were dissociated with ethylenediaminetetraacetic acid (EDTA, Lonza) for 1-2 min at 37°C and seeded in a 6-well plate at a density of 1×10^5 cells per well. Detachment of iPSCs to obtain embryoid bodies requires dispase (Thermo Fisher Scientific) to begin the process of neural differentiation; the bodies were then cultured in neural induction medium containing N2 supplement (Thermo Fisher Scientific), nonessential amino acids (MEM-NEAA, Thermo Fisher Scientific) and DMEM/F12 (Thermo Fisher Scientific) for 7 days. On day 7, EBs were resuspended in Matrigel (Corning), which was pipetted cold in 3-mm dimples on a sheet of Parafilm that was sterilized by UV for 30 min. These droplets solidified at 37°C and were subsequently removed from the Parafilm and grown in differentiation medium that was changed every 5 days.

Genome editing. DS iPSC lines with DSCAM knockdown were generated by CRISPR/Cas9. Exon 1 of DSCAM was selected for guide RNA (gRNA) design according to the CRISPR online

design tool at http://crispr.mit.edu/. The DSCAM gRNA sequences of a pair of oligos for the targeting site are as follows: forward, 5′-CAG GCG ATG AAA GAC GTG AAA TGT-3′; reverse, 5′-AAC CAT GAG AGG CAA TGT TG-3′. After transformation and extraction of the plasmid, 15 μg of gRNA-containing plasmid was transferred to 50000 DS1 cells using an electroporation apparatus (Lonza). After 24 hours of electroporation, puromycin was added to the cell cultures for 2 days. At 3-4 days after electroporation, single clones were picked and reseeded in a 24-well plate. Knockdown of the DSCAM gene was verified by sequencing, and two iPSC lines—DSCAM-KD^{2-1-12} and DSCAM-KD^{2-1-6}—were obtained. As knockdown groups, DSCAM-KD^{2-1-12} and DSCAM-KD^{2-1-6} were used to verify the molecular mechanism related to the DSCAM-PAK1 pathway during cortical development.

Immunostaining. Organoids were fixed with 4% paraformaldehyde for 2 hours in an Eppendorf tube. After they were washed with phosphate-buffered saline (PBS) for 10 min three times, the organoids were submerged in 20% sucrose in PBS overnight at 4°C. After the organoids sank to the bottom of the tube, the soaking solution was replaced by 30% sucrose in PBS at 4°C. Organoids were embedded in optimal cutting temperature (OCT) compound and cryosectioned at 10 μm. Tissue sections were then used for immunostaining. For immunohistochemistry, sections were washed with PBS 3 times and then blocked and permeabilized in 1% Triton (Biolink) and 5% donkey serum (Millipore) in PBS. Organoids were incubated at 4°C overnight in primary antibody (detailed list in Supplemental Table 2) diluted in 0.2% Triton and 5% donkey serum. On the second day, organoids were incubated for 1 hour at 20°C in secondary antibody diluted in 5% donkey serum. After treatment with primary and secondary antibodies (detailed list in Supplemental Table 2), three

10-minute washes in PBS were performed. Coverslips were mounted for fluorescent imaging. Images were acquired using an Eclipse 80i fluorescence microscope.

EdU Click-iT assay. Organoids were kept in neural induction medium with EdU (10 μM, Life Technologies) for 2 hours. Then, the neural induction medium was discarded before the organoids were fixed with 4% paraformaldehyde for 2 hours at room temperature. After they were washed with 3% bovine serum albumin (BSA) twice, the organoids were maintained in 0.5% Triton for 20 min at 20°C, after which an EdU Click-iT assay was performed per the manufacturer's instructions (Invitrogen, C10338), followed by immunostaining.

Western blotting. Organoids were lysed in RIPA buffer containing protease and protease inhibitor cocktail (Roche). Proteins were loaded into gels (SurePage) and separated by SDS-PAGE with 100 V electrophoresis. Then, proteins were transferred to polyvinylidene fluoride membranes at 300 mA for 2 hours and blocked in 5% skim milk for 2 hours at room temperature. Primary antibodies (detailed list in Supplemental Table 2) were incubated overnight at 4°C before the membranes were washed with 8× PBST solution five times for 8 min the next day. The secondary antibodies were incubated with the membranes on a shaker for 2 hours at room temperature. After the incubation was completed, the secondary antibody was decanted, and the membranes were again washed 5 times with 1× PBST for 8 min. Anti-GAPDH was used as an internal reference and loading control. Horseradish peroxidase-conjugated immunoglobulin G was used as the secondary antibody, and the ECL system was used for detection of the protein bands. The luminol substrate solutions A and B were mixed at a volume of 1:1 and then added to the surface of the membrane in the dark.

After 1 min, the protein bands were exposed over a time gradient.

Bulk RNA sequencing, ATAC sequencing and bioinformatics analysis. Following a standard protocol, total RNA from day 30 trisomy 21 and euploid organoids was extracted using a TRIzol reagent kit (Invitrogen, Carlsbad, CA, USA). RNA integrity was checked on an Agilent 2100 BioAnalyzer to conduct quality control (Agilent Technologies, Santa Clara, CA, USA). Library construction and high-throughput RNA sequencing (RNA-seq) were performed with the HiSeqTM 4000 sequencing platform (Illumina, California, USA). RNA-seq reads were aligned to the human reference genome (GRCh37/hg19) by using HISAT2 software (v.2.1.0.) (54).

The gene abundances were calculated and normalized as the TPM (transcripts per million). We determined DEGs between the trisomy 21 and euploid groups by using the DESeq2 (55) package (v.1.30.0). Enriched GO terms were identified with MGI Gene Ontology Term Finder (http://www.informatics.jax.org/gotools/MGI_Term_Finder.html). A log2 (fold change) ≥ 1 and P-value < 0.05 were used as thresholds. Protein-protein interaction (PPI) network analysis of the differentially expressed proteins was performed using STRING v.10.0a software.

For ATAC-seq, organoids were dissociated into a single-cell suspension. Approximately 50000 single cells from each group were used for nuclei prep. First, we spun cells for 5 min at 500× g and 4°C, and then we washed these cells once with 50 µl of cold 1x PBS buffer before another centrifugation step for 5 min at 500 ×g and 4°C. Next, cells were lysed in 50 µl of cold lysis buffer (10 mM Tris-HCl, pH 7.4; 10 mM NaCl; 3 mM MgCl2 and 0.1% IGEPAL CA-630) on ice, and nuclei were pelleted by centrifugation at 500 ×g for 10 min. We collected nuclei, resuspended them in 50 µl of transposase reaction mix from a Nextera DNA Sample Preparation Kit (Illumina) and

incubated the reaction at 37°C for 30 min to carry out the Tn-5 transposition reaction. Then, we purified DNA fragments using a MinElute PCR Purfication Kit (Qiagen). Transposed DNA fragments were then amplified using the following PCR conditions: 1 cycle of 72°C for 5 min and 98°C for 30 s and 10 cycles of 98°C for 10 s, 63°C for 30 s and 2°C for 2 min. Subsequently, the resulting ATAC-seq libraries were purified (MinElute Kit, Qiagen) and 150-bp paired-end sequenced on the Illumina Nova 6000 platform to a depth of 4.0×10^7 reads.

ATAC-seq data were then processed after mild modifications (including quality control, trimming, filtering, aligning and peak calling). In brief, FastQC (v.0.11.7, http://www.bioinformatics.bbsrc.ac.uk/projects/fastqc) was used to evaluate the quality of the sequencing data, and reads with a Phred quality score > 30 were used for downstream analysis. For the purpose of obtaining clean data with minimal background noise, we removed and trimmed the adaptor sequences using Trimmomatric. Subsequently, the remaining clean reads were aligned to the hg38 reference genome using Burrows-Wheeler Aligner (BWA) software. Samtools (v.1.3.1) was applied to filter out multiple mapped reads, and BED tools were used to filter out mitochondrial reads.

We applied Homer software (4.6; findPeaks-style dnase) and macs2 software with a cut-off Q value < 0.05 to identify peaks, determine peak position and distribution on the genome, identify peak-associated genes, and discover de novo binding motifs.

Differential peaks between trisomy 21 organoids and euploid organoids were identified by DESeq2 (55), with the thresholds of |log2FC| > 1 and P-value < 0.05. Genome-wide normalized signal coverage tracks were created by bamCoverage in deepTools (version 3.3.0) and were visualized in the Integrative Genomics Viewer (IGV version 2.5.0). GO enrichment analysis of the genes

associated with ATAC-seq peaks was performed using clusterProfiler (3.10.1) (56). Fisher's exact test was applied to identify the significant GO categories, and the false discovery rate (FDR) was adopted to correct the p-values.

Dissociation of brain organoids and single-cell RNA-seq. Day 30 and day 70 organoids derived from trisomy 21, euploid, and DSCAM-KD iPS cell lines were prepared for scRNA-seq (sample information is listed in Supplementary Table 3). Briefly, 5-7 cerebral organoids were dissociated into a single-cell suspension via incubation with 1 ml of tryp-LE (Life Technology) for 35 min at 37°C with gentle agitation every 5-8 min, 3 washes with 2% fetal bovine serum (FBS) in DPBS 3, and gentle titration using a P200 pipette. A single-cell suspension was subsequently collected into 1.5 ml microtubes at a cell density of 1000 cells/μl, and approximately 12,000 cells in each channel were loaded onto a Chromium Single Cell 3′ Chip (10x Genomics, PN-120236) and processed through a Chromium controller to generate single-cell gel beads in emulsions (GEMs) according to the manufacturer's instructions. Captured cells were lysed, and the released RNA was barcoded through reverse transcription in individual GEMs. Reverse transcription was performed on a S1000TM Touch Thermal Cycler (Bio Rad) at 53°C for 45 min, followed by 85°C for 5 min and final hold at 4°C. cDNA was generated and then amplified, and quality was assessed using an Agilent 4200. scRNA-seq libraries were prepared with the Chromium Single Cell 3′ Library & Gel Bead Kit V3 (10x Genomics, 1000075) and then sequenced on an Illumina NovaSeq6000 with a sequencing depth of at least 750000 reads per cell with a paired-end 150 bp (PE150) reading strategy.

Data analysis for single-cell RNA-seq. Reads were aligned to the hg38 human reference

genome, and gene-level unique molecular identifier (UMI) counts were obtained using Cell Ranger (version 3.1.0). The expression matrix was processed with Seurat (version 3.1.5) (57). The criteria to select cells for subsequent analysis were as follows: 547 < UMIs per cell < 18040, 398 < detected genes < 4849, and mitochondrial transcript proportion < 0.1731563. Sctransform normalization was applied to each Seurat object to control confounding sources of variations such as sequencing depth and mitochondrial fraction (58). In addition, the integration of single-cell data was performed to correct the batch effect. Expression matrices are summarized by the top 14 principal components. Visualization of transcriptomic profiles was conducted by UMAP. The Louvian modularity optimization algorithm was applied to iteratively group cells together into clusters. Cell clusters were annotated to known biological cell types using canonical cell marker genes. Identifying DEGs in trisomy 21 organoids compared to euploid organoids in each cluster was performed using the MAST (version 1.14.0) package (59). The following model was fit with MAST:

zlm (~ group + time, sca, ebayes=TRUE).

Multiple hypothesis testing corrections was performed with the Bonferroni and Holm corrections (60). GO enrichment and KEGG enrichment of DEGs were performed using ToppGene (https://toppgene.cchmc.org/) (61), and the results were visualized with R. Developmental trajectory analysis was performed using slingshot (version 1.4.0) with default parameters (62). Unbiased spatial mapping of all clusters was performed using VoxHunt. The transcriptome profiles were compared with BrainSpan, the largest dataset containing the postmortem developmental human brain atlas (63).

Generation of DSCAM-KD iPSC lines by using CRISPRi. The CRISPRi dual-vector was

packaged in lentivirus to establish the CRISPRi-based DSCAM-KD human iPSC line. First, the lentiviral vector containing dCas9-KRAB used for this study was modified from the lentiCRISPR vector (#61425) obtained from Addgene, with the dCas9-VP64 cassette replaced by dCas9-KRAB. We then designed sgRNAs targeting the DNA region from –50 to 300 bp near the transcription start site (TSS) of the DSCAM gene and used the web tool http://crispr.mit.edu/to minimize off-target effects of the sgRNAs. The location of the TSS was determined using NCBI (http://www.ncbi.nlm.nih.gov/). Three gRNAs targeting DSCAM as well as a non-targeting negative control gRNA were selected (Supplemental Table 4) using the online CRISPR design tool (https://bioinfogp.cnb.csic.es/tools/breakingcas/); these sequences were cloned into the hU6-sgRNA-SV40-EGFP vector (GeneChem Technologies, #GV371).

For the dual-vector multiplex experiments, human iPSCs from DS1 were first infected with lentivirus expressing dCas9-KRAB at 3 days after mechanical passage for 24 hours. Selection was applied 7 days postinfection with blasticidin (1 μg/ml) in E8 medium in the presence of the ROCK inhibitor Y27632 (2 μM) (STEMCELL Technologies, Vancouver, Canada) and then persistently cultured in the presence of 0.2 μg/ml blasticidin at 13 days postinfection to maintain the selection, which was continued for 5 weeks until stable colonies appeared. A second transduction in clones was performed using lentivirus encoding either targeting or scramble sgRNA. Twenty-four hours after lentiviral infection, the cell culture medium was replaced with E8 medium supplemented with ROCK inhibitor (STEMCELL Technologies, Vancouver, Canada). At 14 days postinfection, cells were dissociated with Accutase treatment for 10 min at 37°C to create a single-cell suspension; this suspension was then transferred to a 5 ml flow cytometry tube with a strainer cap before FACS purification could be completed on a BD FACS Aria Fusion instrument. Clones were then expanded

into larger vessel formats and used for further experiments, including functional CRISPRi activity and organoid differentiation.

Real-time PCR. All RNA samples were extracted by using a TRIzol kit (Thermo Fisher Scientific). One microgram of total RNA from each sample was reverse transcribed into cDNA and then subjected to real-time PCR using SuperScript III First-Strand (Thermo Fisher Scientific). Primers for real-time PCR were as follows: DSCAM, forward primer CCA GGC TCA GGT AAT CTCA and reverse primer, AGC ATA GTC TGT GTT CCGA; and PAK1, forward primer CAG CCC CTC CGA TGA GAA ATA; and reverse primer CAA AAC CGA CAT GAA TTG TGT GT.

Cytogenetic analysis. Cerebral organoids were collected for cell culture followed by karyotyping. GTG banding was performed according to a standard protocol. Karyotypes were determined from G-banding analysis using a standard protocol according to the ISCN 2016 nomenclature.

Quantification of neural tubes in organoids and statistical analysis. Organized portions of the organoids around the VZ-like structure were the target area for quantification of neural tubes in organoids. The image was rotated such that the VZ-like region was horizontal. Then, a box was defined with a specific width but flexible height to cover the entire stratified region from the apical surface of the VZ to the top surface of the organoid. All Hoechst-stained cells and cells expressing the target markers within that box were counted for statistical analysis. Organoids from the same experiment and from the same clone but from independent experiments were used as technical

replicates. The data were averaged to obtain a single value. Average data from different biological replicates from different individuals were used to determine the average and standard error.

Data availability. The raw data of single-cell RNA-seq data, bulk RNA-seq data, ATAC-seq data used in this study have been deposited in the Sequence Read Achieve (SRA) of NCBI under the accession number (SRR14243996-SRR14244067).

Statistics. All data represent means ± SEM. All statistical analyses and graphing were done using GraphPad Prism software (GraphPad Software, La Jolla, CA, USA; version 8). Statistical methods relevant to each figure are described in the figure legends. Statistical comparisons between two groups were performed by Student's t test. Other statistical analyses were performed using one-way ANOVA (with Dunnett's multiple comparisons test). P values less than 0.05 were considered to indicate a significant difference between groups.

Study approval. H9 and IMR90-4 cell line were obtained from Wicell Agreeement (H9: NO.16-W0060; IMR90-4: NO.17-W0063); DS1, 2DS3, DSP and DS2U cell lines were gifts of Bhattacharyya laboratory (Department of Cell and Regenerative Biology and Neuroscience University of Wisconsin, Madison, WI, USA). ihtc-03 cell line was established in our laboratory(35), verbal and written consent of generation and differentiation of the ihtc-03 cell line was obtained from participant. The study was approved by the ethic community of Nanjing Medical University ([2016]NO.326).

Author contributions

XYT and YL designed the experiment. XYT, LX, ML, JW, AB, and YL wrote the manuscript. XYT and LX performed the experiments with technical assistance from XG, QZ, CYL, DW, KHF, MX, XH, SW, XW, XYT, YH, and XYZ. ML, JW and YH performed RNA-seq analyses and scRNA-seq analysis. ML, XYT, YW, and YH performed ATAC-seq analyses. XYT and YL performed additional data analyses. YL directed the project.

Acknowledgements

This study was supported by the Strategic Priority Research Program of the Chinese Academy of Sciences (Grant No. XDA16010306), the National Natural Science Foundation of Chinese Grants (81922022, 91849117, 81471301 and 81701320), the National Key Research and Development Program of China (2019YFA0802703), the Jiangsu Outstanding Young Investigator Program (BK20160044), and the Jiangsu Province's Innovation Program.

References

1. Hibaoui Y, et al. Modelling and rescuing neurodevelopmental defect of Down syndrome using induced pluripotent stem cells from monozygotic twins discordant for trisomy 21. *EMBO Mol Med.* 2014;6(2):259-77.
2. Golden JA, and Hyman BT. Development of the superior temporal neocortex is anomalous in trisomy 21. *J Neuropathol Exp Neurol.* 1994;53(5):513-20.
3. Chakrabarti L, Galdzicki Z, and Haydar TF. Defects in embryonic neurogenesis and initial synapse formation in the forebrain of the Ts65Dn mouse model of Down syndrome. *J Neurosci.* 2007;27(43):11483-95.
4. Schapiro MB, et al. Serial quantitative CT analysis of brain morphometrics in adult Down's syndrome at different ages. *Neurology.* 1989;39(10):1349-53.
5. Coyle JT, Oster-Granite ML, and Gearhart JD. The neurobiologic consequences of Down syndrome. *Brain Res Bull.* 1986;16(6):773-87.
6. Wisniewski KE. Down syndrome children often have brain with maturation delay, retardation of growth, and cortical dysgenesis. *Am J Med Genet Suppl.* 1990;7:274-81.
7. Lu J, et al. OLIG2 over-expression impairs proliferation of human Down syndrome neural progenitors. *Hum Mol Genet.* 2012;21(10):2330-40.
8. Bahn S, et al. Neuronal target genes of the neuron-restrictive silencer factor in neurospheres derived from fetuses with Down's syndrome: a gene expression study. *Lancet.* 2002;359(9303):310-5.
9. Bhattacharyya A, et al. A critical period in cortical interneuron neurogenesis in down syndrome revealed by human neural progenitor cells. *Dev Neurosci.* 2009;31(6):497-510.
10. Bhattacharyya A, and Svendsen CN. Human neural stem cells: a new tool for studying cortical

development in Down's syndrome. *Genes Brain Behav.* 2003;2(3):179-86.

11. Weick JP, et al. Deficits in human trisomy 21 iPSCs and neurons. *Proc Natl Acad Sci U S A.* 2013;110(24):9962-7.
12. Huo HQ, et al. Modeling Down Syndrome with Patient iPSCs Reveals Cellular and Migration Deficits of GABAergic Neurons. *Stem Cell Reports.* 2018;10(4):1251-66.
13. Watanabe M, et al. Self-Organized Cerebral Organoids with Human-Specific Features Predict Effective Drugs to Combat Zika Virus Infection. *Cell Rep.* 2017;21(2):517-32.
14. Lancaster MA, et al. Cerebral organoids model human brain development and microcephaly. *Nature.* 2013;501(7467):373-9.
15. Mariani J, et al. FOXG1-Dependent Dysregulation of GABA/Glutamate Neuron Differentiation in Autism Spectrum Disorders. *Cell.* 2015;162(2):375-90.
16. Kadoshima T, et al. Self-organization of axial polarity, inside-out layer pattern, and species-specific progenitor dynamics in human ES cell-derived neocortex. *Proc Natl Acad Sci U S A.* 2013;110(50):20284-9.
17. Pasca AM, et al. Human 3D cellular model of hypoxic brain injury of prematurity. *Nat Med.* 2019;25(5):784-91.
18. Amin ND, and Pasca SP. Building Models of Brain Disorders with Three-Dimensional Organoids. *Neuron.* 2018;100(2):389-405.
19. Pasca SP. Assembling human brain organoids. *Science.* 2019;363(6423):126-7.
20. Bershteyn M, et al. Human iPSC-Derived Cerebral Organoids Model Cellular Features of Lissencephaly and Reveal Prolonged Mitosis of Outer Radial Glia. *Cell Stem Cell.* 2017;20(4):435-49.e4.

21. Iefremova V, et al. An Organoid-Based Model of Cortical Development Identifies Non-Cell-Autonomous Defects in Wnt Signaling Contributing to Miller-Dieker Syndrome. *Cell Rep.* 2017;19(1):50-9.

22. Qian X, et al. Sliced Human Cortical Organoids for Modeling Distinct Cortical Layer Formation. *Cell Stem Cell.* 2020;26(5):766-81.e9.

23. Bowers M, et al. FASN-Dependent Lipid Metabolism Links Neurogenic Stem/Progenitor Cell Activity to Learning and Memory Deficits. *Cell Stem Cell.* 2020;27(1):98-109.e11.

24. Yoon KJ, et al. Zika-Virus-Encoded NS2A Disrupts Mammalian Cortical Neurogenesis by Degrading Adherens Junction Proteins. *Cell Stem Cell.* 2017;21(3):349-58.e6.

25. Khan TA, et al. Neuronal defects in a human cellular model of 22q11.2 deletion syndrome. *Nat Med.* 2020;26(12):1888-98.

26. Johnstone M, et al. Reversal of proliferation deficits caused by chromosome 16p13.11 microduplication through targeting NFκB signaling: an integrated study of patient-derived neuronal precursor cells, cerebral organoids and in vivo brain imaging. *Mol Psychiatry.* 2019;24(2):294-311.

27. Wang L, et al. Loss of NARS1 impairs progenitor proliferation in cortical brain organoids and leads to microcephaly. *Nat Commun.* 2020;11(1):4038.

28. Xiang Y, et al. Dysregulation of BRD4 Function Underlies the Functional Abnormalities of MeCP2 Mutant Neurons. *Mol Cell.* 2020;79(1):84-98.e9.

29. Miura Y, et al. Generation of human striatal organoids and cortico-striatal assembloids from human pluripotent stem cells. *Nat Biotechnol.* 2020;38(12):1421-30.

30. Jia YL, et al. Expression and significance of DSCAM in the cerebral cortex of APP transgenic mice. *Neurosci Lett.* 2011;491(2):153-7.

31. Chen BE, et al. The molecular diversity of Dscam is functionally required for neuronal wiring specificity in Drosophila. *Cell.* 2006;125(3):607-20.

32. Perez-Nunez R, et al. Overexpressed Down Syndrome Cell Adhesion Molecule (DSCAM) Deregulates P21-Activated Kinase (PAK) Activity in an In Vitro Neuronal Model of Down Syndrome: Consequences on Cell Process Formation and Extension. *Neurotox Res.* 2016;30(1):76-87.

33. Pan X, et al. PAK1 regulates cortical development via promoting neuronal migration and progenitor cell proliferation. *Mol Brain.* 2015;8:36.

34. Lancaster MA, and Knoblich JA. Generation of cerebral organoids from human pluripotent stem cells. *Nat Protoc.* 2014;9(10):2329-40.

35. Yuan F, et al. Induction of human somatostatin and parvalbumin neurons by expressing a single transcription factor LIM homeobox 6. *Elife.* 2018;7.

36. Liu Y, et al. Directed differentiation of forebrain GABA interneurons from human pluripotent stem cells. *Nat Protoc.* 2013;8(9):1670-9.

37. Liu Y, et al. Medial ganglionic eminence-like cells derived from human embryonic stem cells correct learning and memory deficits. *Nat Biotechnol.* 2013;31(5):440-7.

38. Zhang X, et al. Local and global chromatin interactions are altered by large genomic deletions associated with human brain development. *Nat Commun.* 2018;9(1):5356.

39. Caviness VS, Jr., Takahashi T, and Nowakowski RS. Numbers, time and neocortical neuronogenesis: a general developmental and evolutionary model. *Trends Neurosci.* 1995;18(9):379-83.

40. Inglis-Broadgate SL, et al. FGFR3 regulates brain size by controlling progenitor cell proliferation and apoptosis during embryonic development. *Dev Biol.* 2005;279(1):73-85.

41. Saito Y, et al. The developmental and aging changes of Down's syndrome cell adhesion molecule

expression in normal and Down's syndrome brains. *Acta Neuropathol.* 2000;100(6):654-64.

42. Alves-Sampaio A, Troca-Marín JA, and Montesinos ML. NMDA-mediated regulation of DSCAM dendritic local translation is lost in a mouse model of Down's syndrome. *J Neurosci.* 2010;30(40):13537-48.
43. Amano K, et al. Dosage-dependent over-expression of genes in the trisomic region of Ts1Cje mouse model for Down syndrome. *Hum Mol Genet.* 2004;13(13):1333-40.
44. Guedj F, et al. Analysis of adult cerebral cortex and hippocampus transcriptomes reveals unique molecular changes in the Ts1Cje mouse model of down syndrome. *Brain Pathol.* 2015;25(1):11-23.
45. Xu R, et al. OLIG2 Drives Abnormal Neurodevelopmental Phenotypes in Human iPSC-Based Organoid and Chimeric Mouse Models of Down Syndrome. *Cell Stem Cell.* 2019;24(6):908-26.e8.
46. Wisniewski KE, Laure-Kamionowska M, and Wisniewski HM. Evidence of arrest of neurogenesis and synaptogenesis in brains of patients with Down's syndrome. *N Engl J Med.* 1984;311(18):1187-8.
47. Ross MH, Galaburda AM, and Kemper TL. Down's syndrome: is there a decreased population of neurons? *Neurology.* 1984;34(7):909-16.
48. Guihard-Costa AM, et al. Biometry of face and brain in fetuses with trisomy 21. *Pediatr Res.* 2006;59(1):33-8.
49. Korbel JO, et al. The genetic architecture of Down syndrome phenotypes revealed by high-resolution analysis of human segmental trisomies. *Proc Natl Acad Sci U S A.* 2009;106(29):12031-6.
50. Lyle R, et al. Genotype-phenotype correlations in Down syndrome identified by array CGH in 30 cases of partial trisomy and partial monosomy chromosome 21. *Eur J Hum Genet.* 2009;17(4):454-66.

51. Yamakawa K, et al. DSCAM: a novel member of the immunoglobulin superfamily maps in a Down syndrome region and is involved in the development of the nervous system. *Hum Mol Genet.* 1998;7(2):227-37.

52. Zhang L, et al. DSCAM and DSCAML1 regulate the radial migration and callosal projection in developing cerebral cortex. *Brain Res.* 2015;1594:61-70.

53. Dolan BM, et al. Rescue of fragile X syndrome phenotypes in Fmr1 KO mice by the small-molecule PAK inhibitor FRAX486. *Proc Natl Acad Sci U S A.* 2013;110(14):5671-6.

54. Kim D, et al. Graph-based genome alignment and genotyping with HISAT2 and HISAT-genotype. *Nat Biotechnol.* 2019;37(8):907-15.

55. Love MI, Huber W, and Anders S. Moderated estimation of fold change and dispersion for RNA-seq data with DESeq2. *Genome Biol.* 2014;15(12):550.

56. Yu G, et al. clusterProfiler: an R package for comparing biological themes among gene clusters. *Omics.* 2012;16(5):284-7.

57. Stuart T, et al. Comprehensive Integration of Single-Cell Data. *Cell.* 2019;177(7):1888-902.e21.

58. Hafemeister C, and Satija R. Normalization and variance stabilization of single-cell RNA-seq data using regularized negative binomial regression. *Genome Biol.* 2019;20(1):296.

59. Finak G, et al. MAST: a flexible statistical framework for assessing transcriptional changes and characterizing heterogeneity in single-cell RNA sequencing data. *Genome Biol.* 2015;16:278.

60. Puoliväli T, Palva S, and Palva JM. Influence of multiple hypothesis testing on reproducibility in neuroimaging research: A simulation study and Python-based software. *J Neurosci Methods.* 2020;337:108654.

61. Chen J, et al. ToppGene Suite for gene list enrichment analysis and candidate gene prioritization.

Nucleic Acids Res. 2009;37(Web Server issue):W305-11.

62. Street K, et al. Slingshot: cell lineage and pseudotime inference for single-cell transcriptomics. *BMC Genomics.* 2018;19(1):477.

63. Kang HJ, et al. Spatio-temporal transcriptome of the human brain. *Nature.* 2011;478(7370):483-9.

Figures and figure legends

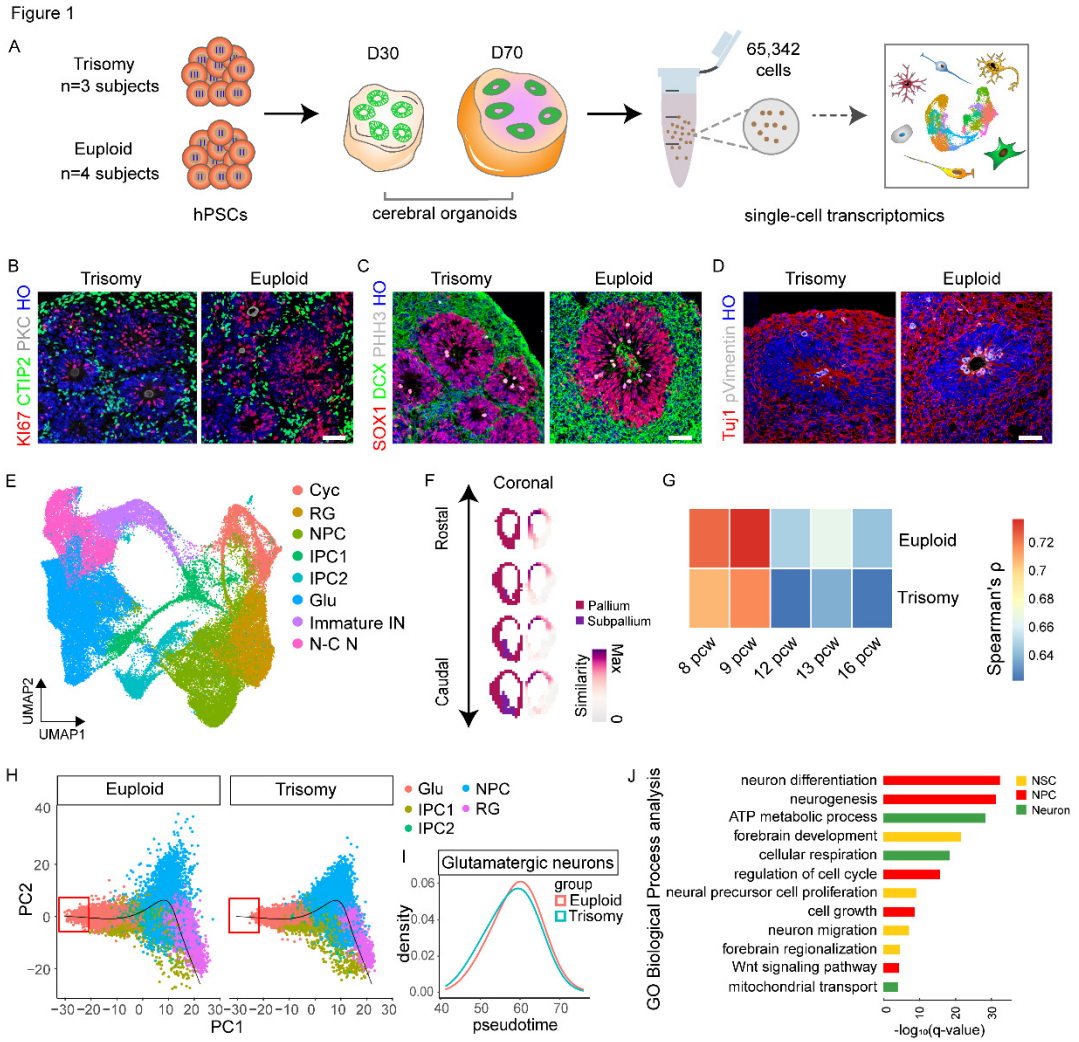

Figure 1. Single-cell transcriptional profiling of cerebral organoids derived from trisomy 21 and euploid human pluripotent stem cell (hPSC) lines. (**A**) Schematic illustrating the generation and analysis of cerebral organoids from trisomy 21 and euploid (3 human iPSC lines from trisomy 21 individuals and 4 euploid hPSC lines). (**B**) Immunofluorescence analysis of cerebral organoids at 30 days after initiation of differentiation shows the proliferation marker Ki67 (red), early-born neuron marker CTIP2 and adherens junction marker PKC (grey) in trisomy 21 and euploid organoids. Scale bar, 50 µm. (**C**) Immunostaining for the neural progenitor marker SOX1 (red), newly born neuron marker DCX and mitotic marker pHH3 (grey) at 30 days of differentiation in trisomy 21 and euploid organoids. Scale bar, 50 µm. (**D**) Representative images of organoids for the neuronal marker Tuj1 (red) and M-phase marker p-vimentin (grey). Scale bar, 50 µm. (**E**) UMAP plot of cell types detected in euploid (n=5) and trisomy (n=4) organoids. Cyc, cycling; RG, radial glial cells; NPC, neural progenitor cells; IPC, intermediate progenitor cells; Glu: glutamatergic neurons; Immature IN, immature inhibitory neurons; N-C N, non-committed neurons. (**F**) VoxHunt spatial brain mapping of all the clusters in the cerebral organoids onto data from E13.5 mouse brains from the Allen Brain Institute. Coronal sections are visualized by scaled similarity scores. (**G**) Transcriptome correlation between day 30 organoids and developing neocortex samples from the

BrainSpan Project (pcw 8-16). The mean Spearman correlation coefficients (r) are indicated. (**H**) Developmental trajectories of the major cell types detected in day 30 trisomy 21 and euploid organoids. (**I**) Distributions of glutamatergic neurons in trisomy and euploid organoids over pseudotime. (**J**) Gene ontology (GO) analysis of differentially expressed genes (DEGs) across all cell types between trisomy 21 and euploid organoids. Selected GO terms with a false discovery rate (FDR)< 0.05 are shown. NSC: Neural stem cell; NPC: Neural progenitor cell.

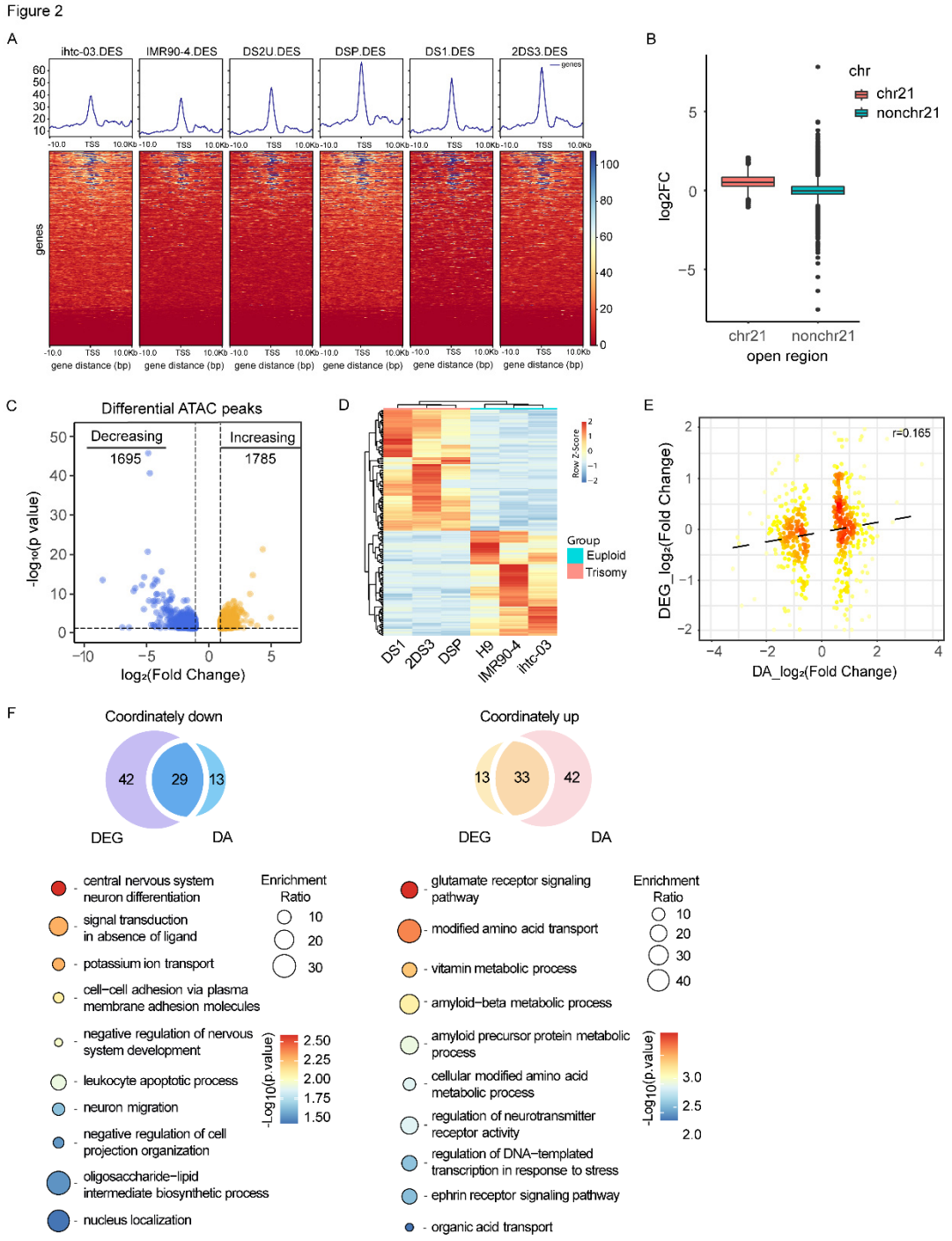

Figure 2. Transcriptional and ATAC-seq analysis in cerebral organoids derived from trisomy 21 and euploid PSCs. (**A**) Heatmaps of regions that are differentially accessible between trisomy

21 and euploid cells at promoter regions on chromosome 21. (**B**) Box plots for log2FC of open chromatin regions (OCRs) among chromosome 21 and other chromosomes. (**C**) Volcano plot of differential ATAC peaks in trisomy 21 cerebral organoids. Differential ATAC peaks were identified by DESeq2. The colour intensity represents the density of the points in the volcano plot. Increased ATAC sites are shown in orange (log2FC > 1 and $p < 0.05$, n =1,785), and decreased ATAC sites are shown in blue (log2FC < -1 and $p < 0.05$, n = 1,695). (**D**) Heatmap of transcriptome analysis shows 193 significantly DEGs in trisomy 21 organoids compared to euploid control organoids with fold change > 2, $q < 0.05$. (**E**) Correlations between gene expression (log2 FC) and chromatin accessibility (log2 FC) are shown. Pearson's correlation coefficients (r) are indicated. FC, fold change. (**F**) GO analysis of the genes showing co-ordinately altered expression and accessibility between trisomy 21 and euploid organoids.

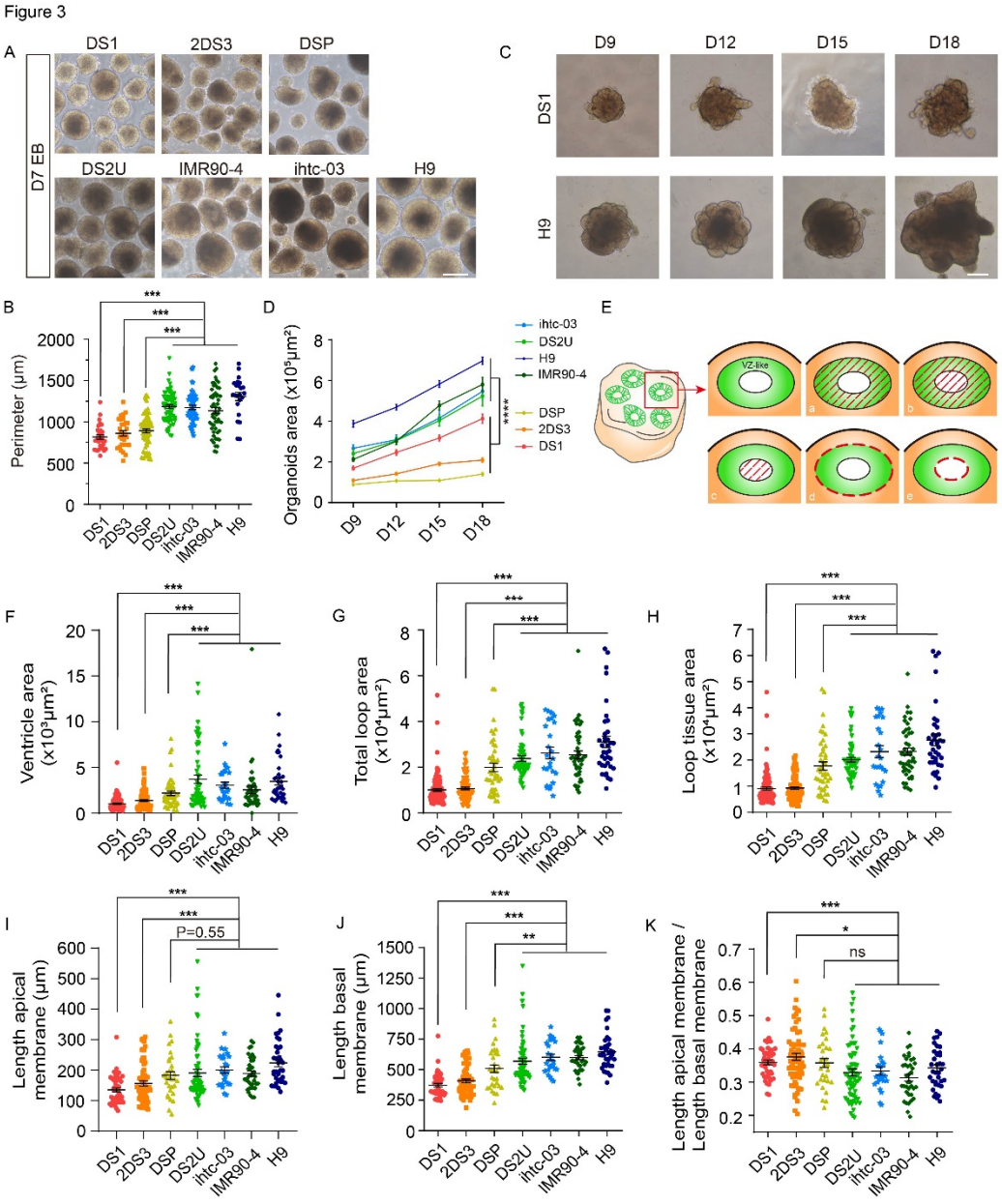

Figure 3. Reduced size and expansion rates of DS patient-derived organoids. (**A**) Bright-field

microscopy images of trisomy 21 and euploid embryonic bodies at day 7. Scale bar, 250 µm. (**B**) Quantification of perimeter at day 7. At least 25 EBs were analysed for each cell line, n ≥3 for independent experiments. Error bars, ± SEM. *P < 0.05, **P< 0.01, ***P < 0.001; one-way ANOVA followed by Dunnett's multiple comparisons test. (**C**) Bright-field microscopy images of trisomy 21 and euploid organoids at different developmental time points. Scale bar, 250 µm. (**D**) Quantification of the organoid area of trisomy 21 and euploid organoids at 9, 12, 15, and 17 days after differentiation reflected a reduction in the expansion rate of trisomy 21 organoids compared to euploid organoids. n ≥16 organoids from three independent biological replicate experiments were analysed for each cell line. Error bars, ± SEM. *P < 0.05, **P< 0.01, ***P < 0.001; two-way ANOVA followed by Sidak's multiple comparisons test. (**E**) Schematic overview of the different parameters of neuroepithelial loops in organoids at 30 days after induction of differentiation. Shown are loop tissue area (a), total loop area (b), ventricle area (c), length basal membrane (d), and length apical membrane (e). (**F-K**) Quantification of a series of parameters in neuroepithelial loops of trisomy 21 and euploid organoids at 30 days. n ≥16 organoids from three independent biological replicate experiments were analysed for each cell line. Error bars, ± SEM. *P < 0.05, **P< 0.01, ***P < 0.001; one-way ANOVA followed by Dunnett's multiple comparisons test.

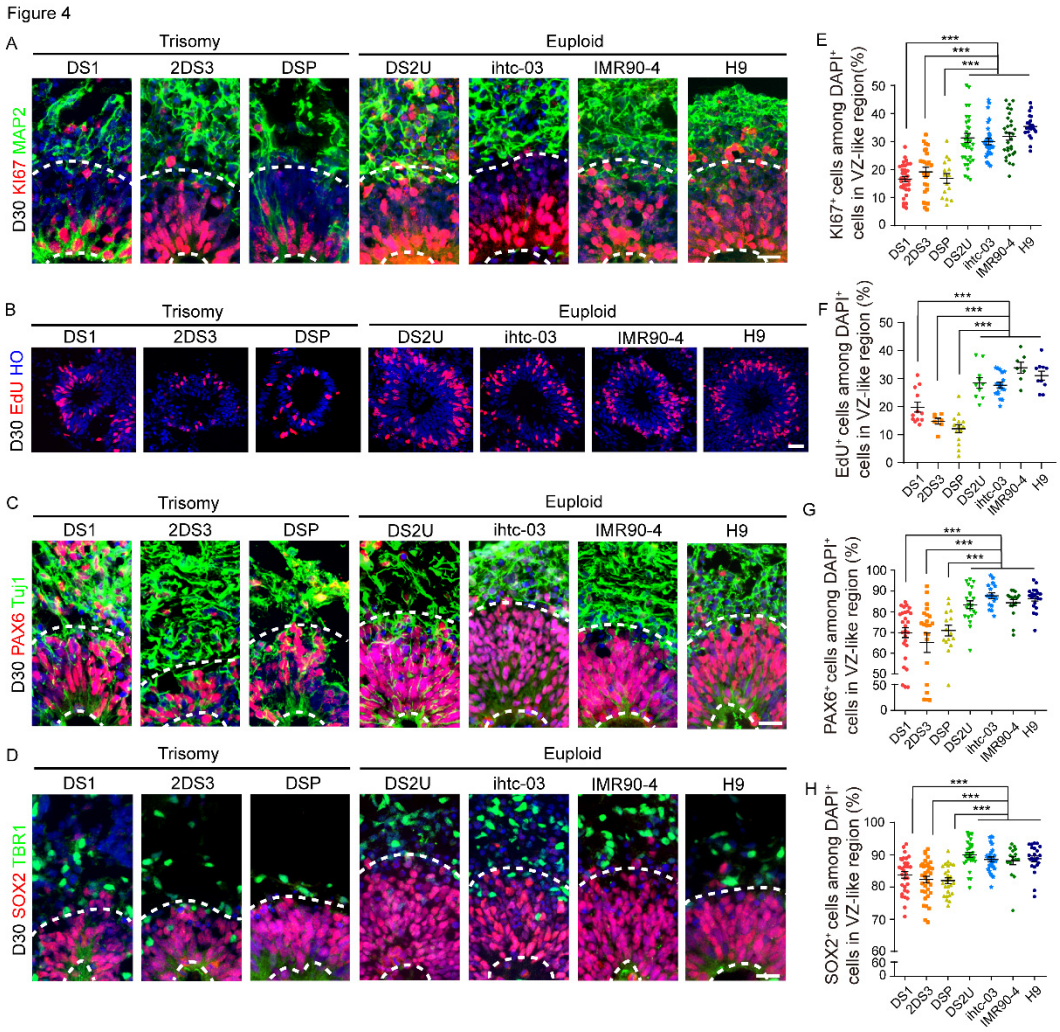

Figure 4. Proliferation studies of 30 days cerebral organoids. (**A-D**) Immunofluorescence of

Ki67$^+$, EdU$^+$, SOX2$^+$ and PAX6$^+$ proliferating RG progenitors, mature MAP2$^+$, TUJ1$^+$ neurons and deep-layer VI TBR1$^+$ excitatory neurons after 30 days of differentiation. Scale bars, 20 µm. (**E-H**) Quantification of the proportion of Ki67$^+$, SOX2$^+$, PAX6$^+$, EdU$^+$ cells in trisomy 21 and euploid organoids after 30 days of differentiation. n=15 to 42 VZ-like regions in at least 5 organoids per cell line were counted. Error bars, ± SEM. *P < 0.05, **P< 0.01, ***P < 0.001; one-way ANOVA followed by Dunnett's multiple comparisons test.

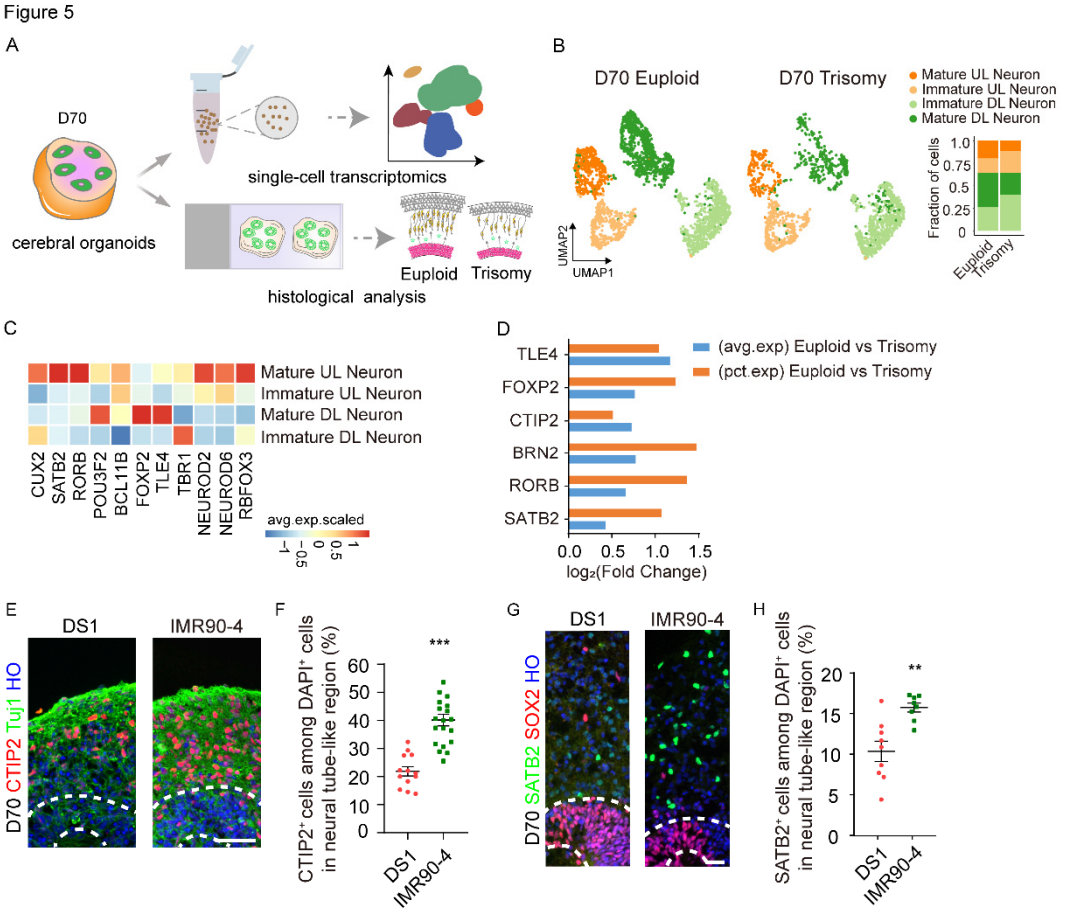

Figure 5. Neurogenesis studies of cerebral organoids. (**A**) Schematic illustrating the single-cell transcriptomic and histological analysis of trisomy 21 and euploid organoids. (**B**) UMAP visualization of single-cell RNA (scRNA) expression in glutamatergic neuron subclusters of trisomy 21 and euploid organoids after 70 days of in vitro differentiation. Bottom right corner bar chart showing the comparisons of cell composition between the trisomy 21 and euploid organoids after 70 days of differentiation. (**C**) Average expression levels of representative markers in each glutamatergic neuron subcluster are visualized by scaled expression scores. (**D**) Histogram of log2 (Fold Change) of average expression and percentage of expression for significantly different genes in the glutamatergic neuron subcluster. (**E**) Decreased mature CTIP2$^+$ neurons at 70 days in trisomy 21 organoids compared to euploid organoids. Scale bar, 50 µm. (**F**) Quantification of the proportion of CTIP2$^+$ cells in both trisomy and euploid organoids at 70 days. (n=13 to 20 neural tube-like regions in at least 5 organoids per cell line were counted; error bars, ±SEM; Student's t test). (**G**) Decreased maturation of SATB2$^+$ neurons at 70 days in trisomy 21 organoids compared to euploid organoids. Scale bar, 25 µm. (**H**) Quantification of the proportion of SATB2$^+$ cells in trisomy and

euploid organoids at 70 days. (n=9 to 11 neural tube-like regions in at least 5 organoids per cell line were counted; error bars, ±SEM; Student's t test).

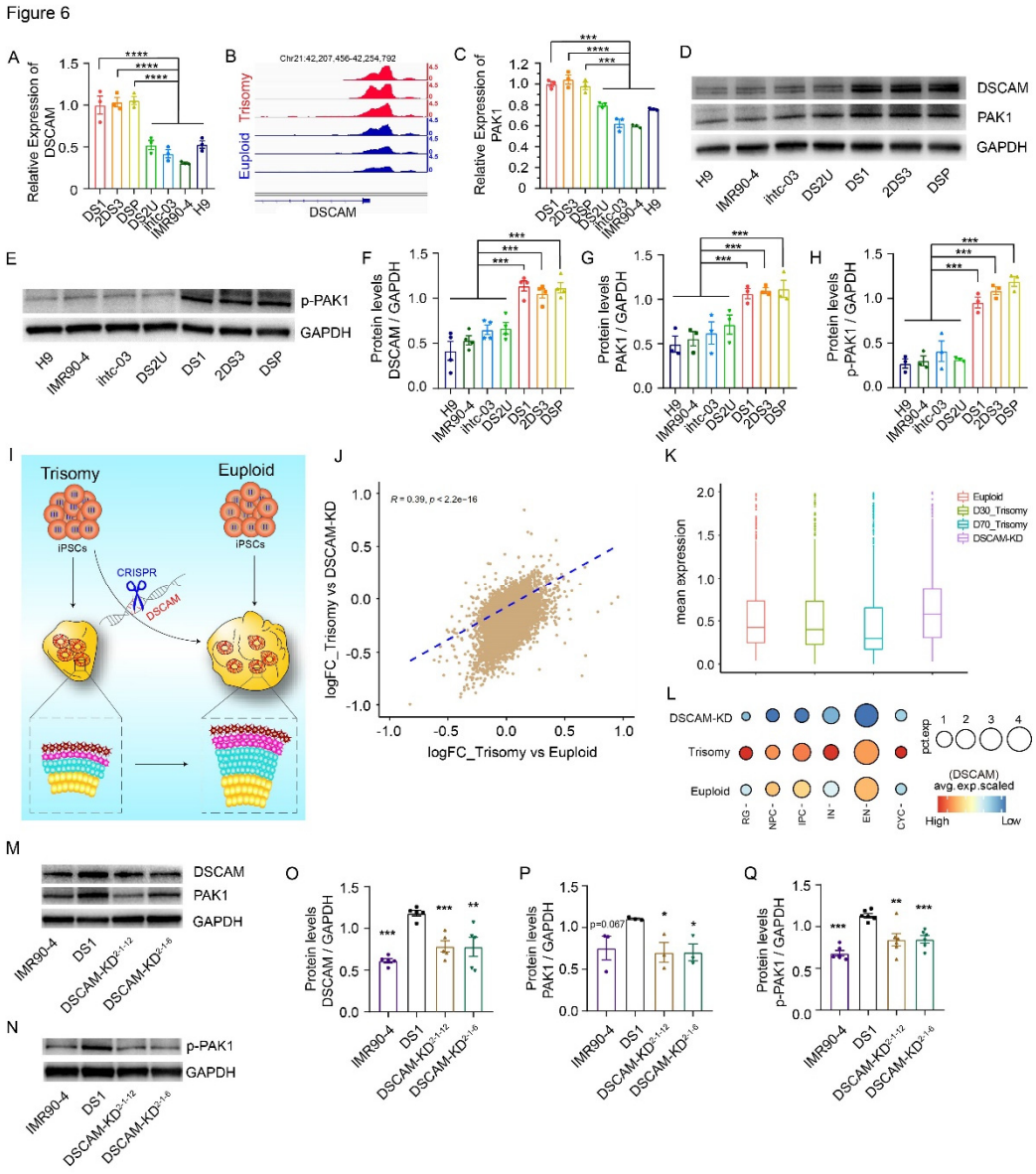

Figure 6. DSCAM-KD rescued impaired DSCAM-PAK1 signalling in DS-derived cortical cultures. (**A**) Relative expression levels of DSCAM in day 30 trisomy 21 and euploid organoids using qPCR. (**B**) Coverage maps of normalized ATAC-seq signals from trisomy 21 and euploid organoids showing a differentially accessible (DA) peak near the DSCAM gene on chromosome 21. (**C**) Relative expression levels of PAK1 in day 30 trisomy 21 and euploid organoids as assessed by qPCR. (**D-E**) Detection of DSCAM, PAK1 and p-PAK1 in trisomy 21 and euploid organoids at 30 days as assessed by western blot. (**F-H**) Representative quantitation of relative DSCAM, PAK1 and p-PAK1 expression in trisomy 21 and euploid organoids. n ≥3 for independent experiments. Error bars, ± SEM; *P < 0.05, **P< 0.01, ***P < 0.001; one-way ANOVA followed by Dunnett's multiple comparisons test. (**I**) Schematic diagram illustrating the effects of DSCAM knockdown on proliferation and neurogenesis in trisomy 21 and euploid cerebral organoids. (**J**) Correlations of the

changes in the expression between trisomy 21 organoids and DSCAM-KD organoids and between trisomy 21 organoids and euploid organoids. Spearman's correlation coefficients (r) are indicated. FC, fold change. (**K**) Boxplot showing the average expression level of the trisomy 21-associated DEGs that were downregulated among trisomy 21-, euploid- and DSCAM-KD cerebral organoids. **(L)** Dot plot showing the DSCAM expression level of multiple clusters among trisomy 21, euploid and DSCAM-KD cerebral organoids. The size of each circle reflects the percentage of cells in a cluster where DSCAM is detected, and the colour intensity reflects the average expression level within each cluster. (**M-N**) Representative western blots of DSCAM, PAK1 and p-PAK1 levels in trisomy 21 and DSCAM-KD organoids. (**O-Q**) Representative relative quantitation of DSCAM, PAK1 and p-PAK1 expression levels in trisomy 21 and DSCAM-KD organoids. n ≥3 for independent experiments. Error bars, ± SEM; *P < 0.05, **P< 0.01, ***P < 0.001.

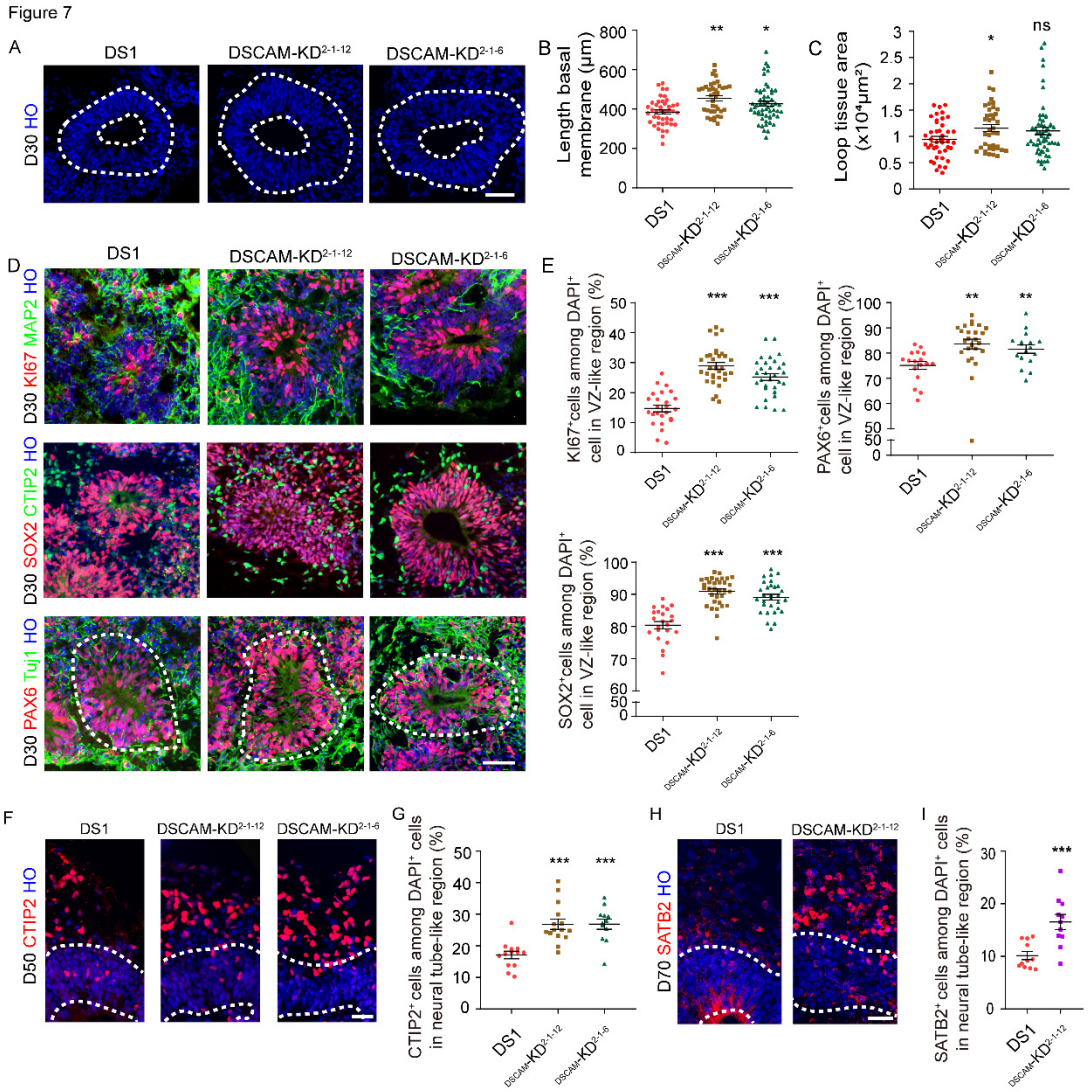

Figure 7. Knocking down DSCAM rescued abnormal neurogenesis in DS-derived cortical cultures. (**A**) Representative images of 30 days organoids stained with Hoechst, which show the quantitation of the different parameters. Scale bar, 50 µm. (**B-C**) Quantitation of the length basal membrane and loop tissue area in the neuroepithelial loops of trisomy 21 and euploid organoids

after 30 days of differentiation. n ≥ 15 organoids from three independent biologic replicate experiments were analysed for each cell line. Error bars, ± SEM; *P < 0.05, **P< 0.01, ***P < 0.001; one-way ANOVA followed by Dunnett's multiple comparisons test. (**D**) Representative images of day 30 trisomy 21 and DSCAM-KD organoids stained for Ki67, SOX2, PAX6, MAP2, CTIP2, and TUJ1 expression. Scale bar, 50 μm. (**E**) Quantification of the proportion of $Ki67^+$, $SOX2^+$, and $PAX6^+$ cells in 30 days trisomy 21 and DSCAM-KD organoids. n=17 to 33 VZ-like regions in at least 10 organoids per cell line were counted. Error bars, ± SEM; *P < 0.05, **P< 0.01, ***P < 0.001; one-way ANOVA followed by Dunnett's multiple comparisons test. (**F-G**) Immunocytochemical staining and quantification of $CTIP2^+$ cells in both trisomy 21 and DSCAM-KD organoids after 50 days of differentiation. n=13 to 15 neural tube-like regions in at least 7 organoids per cell line were counted. Error bars, ± SEM; *P < 0.05, **P< 0.01, ***P < 0.001; one-way ANOVA followed by Dunnett's multiple comparisons test. Scale bar, 35 μm. (**H-I**) Immunocytochemical staining and quantification of the proportion of $SATB2^+$ cells in both trisomy and DSCAM-KD organoids at 70 days. Error bars, ± SEM. (n=11 neural tube-like regions in at least 6 organoids per cell line were counted; error bars, ± SEM; *P < 0.05, **P< 0.01, ***P < 0.001; Student's t test). Scale bar, 35 μm.

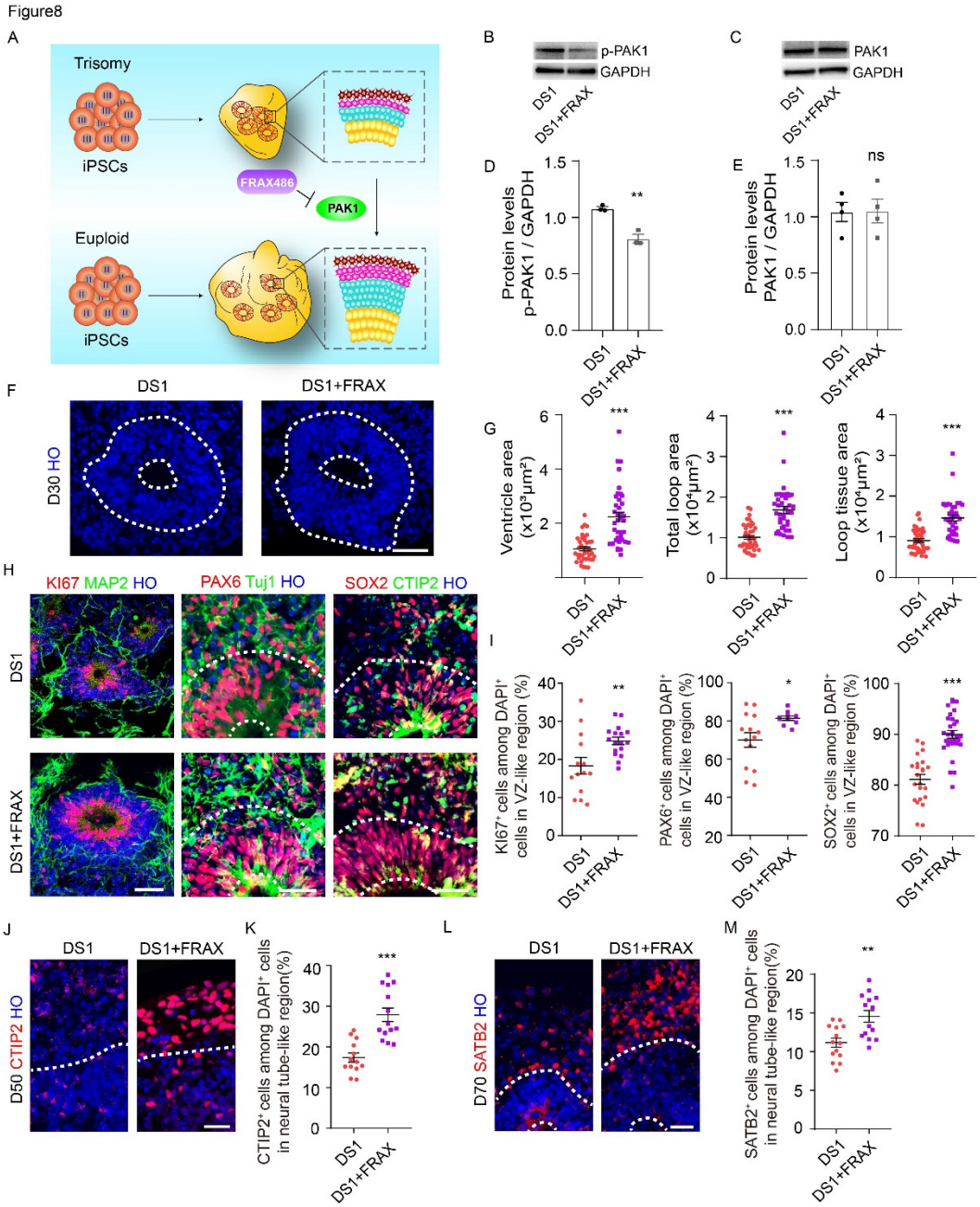

Figure 8. Downregulation of PAK1 rescued proliferation and neurogenesis deficits in DS. (**A**) Graphic design figure of PAK1 correction. (**B-C**) Detection of PAK1 and p-PAK1 in trisomy 21 organoids at 30 days after treatment with FRAX486 by western blot. (**D-E)** Western blot analysis of PAK1 and p-PAK1 in trisomy 21 organoids at 30 days after treatment with FRAX486. (n ≥ 3 for independent experiments; error bars, ± SEM; **P< 0.01; Student's t test). (**F**) Schematic overview of the different parameters in trisomy 21 organoids and rescued organoids at 30 days. Scale bar, 50 µm. (**G**) Quantitation of multiple parameters of neuroepithelial loops in trisomy 21 and rescued organoids. n≥ 10 organoids from three independent biological replicate experiments were analysed for each cell line. Error bars, ± SEM; ***P < 0.001; Student's t test. (**H**) Representative images of trisomy 21 and rescue organoids stained for Ki67, SOX2, PAX6, MAP2, CTIP2, and TUJ1. Scale bars, 20 µm. (**I**) Proportion of Ki67$^+$, SOX2$^+$, and PAX6$^+$ cells in trisomy 21 and rescued organoids

at 30 days. n=10 to 30 VZ-like regions in at least 6 organoids per cell line were counted. Error bars, ± SEM; *P < 0.05, **P< 0.01, ***P < 0.001; Student's t test. (**J-K)** Immunocytochemical staining and quantification of the proportion of $CTIP2^+$ cells in day 50 trisomy 21 and rescued organoids. n=13 to 14 neural tube-like regions in at least 7 organoids per cell line were counted. error bars, ± SEM; ***P < 0.001; Student's t test. Scale bar, 35 μm. (**L-M**) Immunocytochemical staining and quantification of the proportion of $SATB2^+$ cells in day 70 trisomy 21 and rescued organoids. n=9 to 14 neural tube-like regions in at least 6 organoids per cell line were counted. Error bars, ± SEM; **P< 0.01; Student's t test. Scale bar, 35 μm.